Inverse Wing Design and Optimization Using the Euler Flow Equations

Yngve C-J Sedin & Torbjörn Larsson
Saab Military Aircraft
Aerodynamics Department, Computational Aerodynamics
S-581 88 Linköping, Sweden

Abstract

Aerodynamic design, redesign and optimization are key activities when developing efficient fighters and commercial aircraft. The outcome have direct implications on performance, stability and control, fuel consumption and engine exhaust emissions. One very straight forward aerodynamic design procedure is to specify the surface pressure known to improve or gain on flow efficiency and then inversely solve for the unknown geometry. In more advanced applications optimization of drag with constraints involving lift, wing volume or local wing thickness is of interest. This paper presents some results of 3D inverse wing design using an Euler method with a design module based on a fairly simple residual correction relation iteratively up-dating the wing geometry until convergence. Attempts to use the same idea but rearranged for optimization of an objective function including drag are also discussed and preliminary results are shown in 2D. In transonic, using the inverse design method, good agreement was obtained in general with the initially unknown wing. Efforts to impose a given target span loading using inverse design to a 3D wing in supersonic flow is also reported in short.

Introduction

Aerodynamic optimization and shape design are key technologies when developing new fighters or commercial aircraft. Aerodynamic efficiency has an immediate impact on performance, stability and control as well as on fuel consumption and consequently also in the end on environmental aspects. Drag minimization efforts usually involve avoidance of separated regions, reduction of shock wave intensities as well as their secondary interaction on wall boundary layers etc. For fighters controllable high angle attack manoeuvres have come into focus as well as good turn rate performance and mission adapting configurations.

During the last decade Computational Fluid Dynamics (CFD) have made great progress[1]. With present day computers it has become possible even in an industrial environment to regularly use advanced methods based on non-linear flow models like Euler or Navier-Stokes equations. The introduction of more powerful parallel computers in combination with faster and larger memories will further accelerate this development. Certainly the frontier will be pushed forward in the future, towards the use of more inter-disciplinary optimization[2] where aerodynamics will be interactively coupled to other engineering disciplines. In this aerodynamics will play its natural key role as it constitutes the outer physical environment for all vehicles operating in the dense part of the atmosphere.

Design methods for aerodynamic shaping can crudely be divided into two categories[3,4], inverse design and optimization. Traditionally inverse design methods have been attractive to the aerodynamiscist as he or she by physical intuition backed by experience and empirical relations knows how the required pressure distribution should look like. This to avoid viscous separation, diminish shock strength or how to maintain laminar flow on a wing by imposing favourable wing pressures. Inverse methods usually are computationally effective although closure and uniqueness problems may appear when using non-linear flow equations. In using optimization methods, it is not so straight forward to apply skilled experience or physical intuition. The result will be the outcome of how design variables and objective functions are chosen. Uniqueness and dependency on initial data are not always clear. Gradient based methods can be time consuming to apply depending partly on the way of parametrization. One great advantage with optimization procedures is that physical constraints can be imposed to fence in the design within a specified parameter window. This can be difficult to achieve with an inverse design method. For multidisciplinary activities coupled optimization is likely to be the way to go.

This paper presents an efficient inverse design method coupled to an Euler solver. The main idea goes back to the residual correction method of Malone-Narramore-Sankar[5] and Garabedian-McFadden[6]. The Saab development[7,8] was partly carried out during the joint European Union programme called LARA .. An application to a 3D wing design in transonic flow will here be shown as well as some introductory studies in supersonic flow. The simple residual correction relation between geometry and pressure also leads to an idea about aerodynamic shape optimization. Some of these ideas will be outlined and a 2D airfoil optimization will be shown where drag is minimized at constant lift in transonic flow.

Design Method and Flow Solver

The use of Computational Fluid Dynamics (CFD) in the design process requires robust and efficient methods of different complexities partly depending on where in the evolutionary process the development stage is. Sooner or later the baseline concept usually must be aerodynamically improved or redesigned with respect to set overall specifications. In the following the inverse design method IDA (inverse design algorithm) will be described. The inverse module is appended to the Euler module[9] of the 3D Navier-Stokes code MultNas [10] developed at Saab. In fact the IDA module can be used with Navier-Stokes solvers and this has also been successfully tested in 2D.

Inverse design method

The original Garabedian-McFadden[6] residual correction equation was operating in a wrapped-up plane using a complex square root transformation then successively correcting the wing surface in pseudo time adding surface corrections in the mapped space. In this process the pressure deviation residual is the driving right hand side. This was later changed to the modified Garabedian-McFadden[5] (MGM) scheme by working with corrections in the physical space. This approach (Fig 2) was also followed here. Moreover the residual equation may not necessarily be interpreted in pseudo time.

In a Cartesian (x,y,z) frame (see Fig 1) the assumed type of linear relation between geometry and pressure variations can be argued more or less intuitively from physical backgrounds or from perturbation theory. Following this the pressure geometry correction relation was written as follows for lower and upper sides of the wing,

$$F_0\, z + F_1\, z_x + F_2\, z_{xx} + G_1\, z_y + G_2\, z_{yy} = -R^{(upper)}$$
$$F_0\, z + F_1\, z_x + F_2\, z_{xx} + G_1\, z_y + G_2\, z_{yy} = R^{(lower)} \qquad (1)$$

where $z = \Delta Z$ (Fig2) is the geometry correction driven by the pressure coefficient deviation R away from the target

$$R = Cp_{target} - Cp_{current}$$

The from Eq. (1) updated wing geometry, striving to obtain the wished target pressure Cp_{target}, then reads

$$Z = Z_{current} + z$$

The temporary current situation before up-dating is defined by $Z_{current}$ and $Cp_{current}$. So far the scaling coefficients in Eq (1) are assumed to be constants. However they can be modulated by expressions containing the current wing geometry to avoid possible singularities locally in the wing leading edge region.

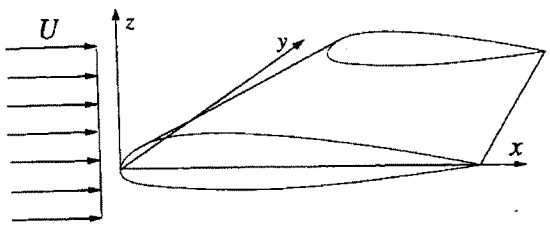

Fig 1. Wing in Cartesian frame of reference (x,y,z)

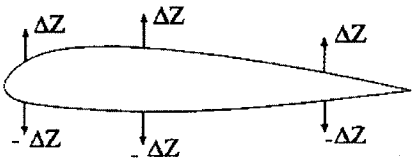

Fig 2. Modified Garabedian-McFadden Method.

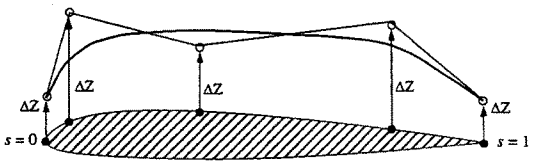

Fig 3. Bezier curve fitting to geometry correction.

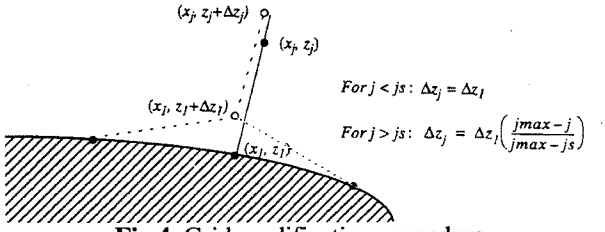

Fig 4. Grid modification procedure.

Before making up the numerical iteration procedure for repeatedly solving Eq(1), it will be further rearranged and split into two separate parts, streamwise and spanwise, in order to simplify the numerical solution as shown below

$$f_0\, z + f_1\, z_x + f_2\, z_{xx} = -c_1\, R^{(upper)}$$
$$g_0\, z + g_1\, z_y + g_2\, z_{yy} = -c_2\, R^{(upper)} \qquad (2)$$
$$f_0\, z + f_1\, z_x + f_2\, z_{xx} = c_1\, R^{(lower)}$$
$$g_0\, z + g_1\, z_y + g_2\, z_{yy} = c_2\, R^{(lower)}$$

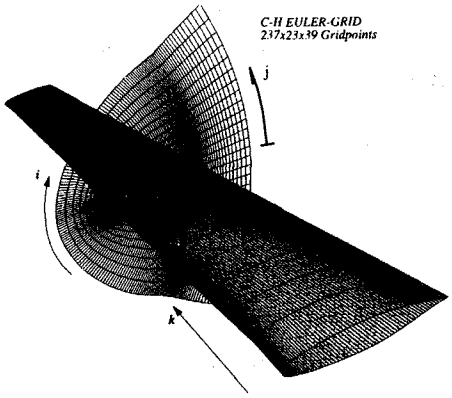

Fig 5. Typical C-H grid topology

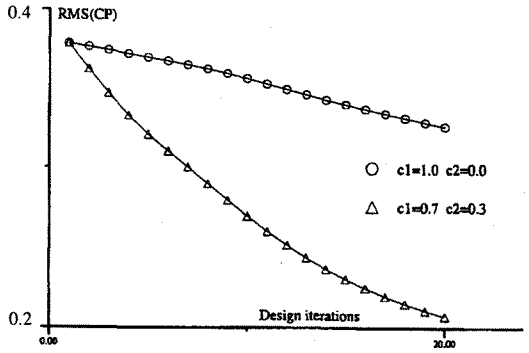

Fig 6. Typical effect of spanwise sweeping on convergence rate of subsonic inverse 3 D wing design .

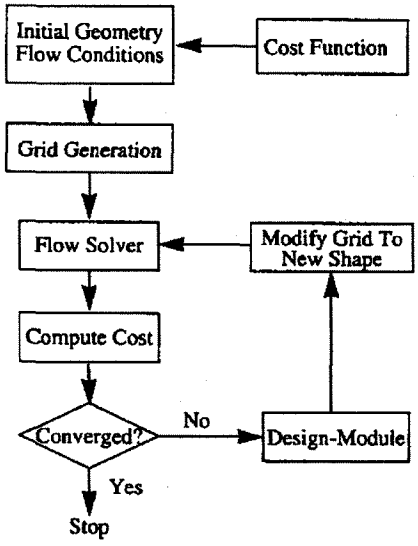

Fig 7. Iterative design (optimization) procedure.

where the weight fractions, streamwise and spanwise, obey $c_1 + c_2 = 1$

The total wing geometry correction up-date then is added up by streamwise and spanwise parts from Eq (2)

$$Z(x,y) = Z_{current} + z^{(streamwise)} + z^{(spanwise)} \qquad (3)$$

The sets of coefficients f_i and g_i of the split system Eq (2) are suitably chosen to achieve stability and convergence in the iterative wing geometry up-dating procedure, Fig 7. On normalising the Eq (2) by the wing mean chord length , $|f_i|$ is usually of order 10, while $|g_i|$ is kept an order of magnitude larger for more under relaxation. The effectiveness of using spanwise sweeping compared to streamwise only is typically shown in Fig 6.

The split system Eq (2) is solved numerically by applying straight forward finite difference approximations with central differences for 2nd order derivatives and one sided "upwind" derivatives simulating 1st order derivatives. This leads to tridiagonal systems of equations of the following types sweeping streamwise *(i)* and spanwise *(k)*

$$A_i z_{i-1} + B_i z_i + C_i z_{i+1} = c_1 R_{i,k}$$
$$A_k z_{k-1} + B_k z_k + C_k z_{k+1} = c_2 R_{i,k} \qquad (4)$$

The tridiagonal coefficients (A_i, B_i, C_i) and (A_k, B_k, C_k) are easily derived applying the above mentioned finite difference approximations to Eq (2) . The grid nodes are the same as those of the wing surface grid built by adjacent cell volumes. With the MGM method, Fig 2, all coefficients only need to be evaluated once. There is only one most forward leading edge point $i = ile$ in each streamwise section and a conductivity condition is imposed there by requiring

$$A_{ile} = 1,\ B_{ile} = -2\ ,\ C_{ile} = 1,\ R_{ile,k} = 0$$

The sweeping of Eq (4) in each wing section is starting at trailing edge lower and ending at trailing edge upper, while the spanwise sweeping is starting in the root symmetry plane ending at the wing tip. As boundary conditions outside the computational domain of Eq (4), zero correction is imposed downstream of the trailing edge and outside the wing tip, while symmetry condition is required across the wing root symmetry plane.

To avoid the wing to start moving vertically without control in the grid (possibly destroying this) one wing geometry point is always kept fixed by adjusting after corrections are added. Moreover, to circumvent fish tail crossover at the trailing edge linear wedges are subtracted.

In order to get smooth solutions Bezier curve fitting (Fig 3) is applied to corrections. Upper and lower sides are separately treated,

in 2 D : $$z(s) = \sum_{i=0}^{n} z_i b_i^n(s) \qquad (5)$$

, where

$$0 \le s \le 1$$

The basis functions $b_i^n(s)$ are described by

$$b_i^n(s) = \binom{n}{i} s^i (1-s)^{n-i} \qquad (6)$$

where $\binom{n}{i}$ are the binomial coefficients.

The number of nodes is n +1 and the description of Eq(5) satisfies the leading and trailing edge values of the sequence z_i . To find the parameter mapping relation s(x) a Newton-Raphson iteration technique is used in each node

$$s^{new} = s^{old} - \frac{x(s^{old})}{x'(s^{old})}$$

The process is started from an initial guess on s and the x(s) and x'(s) are then evaluated from equivalent expressions to Eq(5).

Apart from the Bezier curve fitting a trigonometric interpolation filter can be optionally used.

Now, turning to the successive grid adjustment procedure this is as schematically shown in Fig 4. In the present applications the computational space grid topology is of the C-H type as illustrated in Fig 5. For successively up-dated wing geometries the grid is simply sheared. In each spanwise grid plane along constant *i-lines* but along *j-lines* the grid nodes are vertically shifted in a linear decaying way out to the outer block boundary. Outside this no corrections are made. To avoid grid line crossover close to the wing in cases with highly stretched grids constant vertical corrections are imposed for $j < j_s$, where j_s typically is $j_{max}/2$.

The full inverse design procedure is shown in Fig 7. It starts with an initial wing together with its flow solution and grid. Using the imposed target pressure distribution the process goes on in the inner iteration loop while successively executing the inverse design module and the grid up-dating procedure until the target pressure distribution is sufficiently well satisfied. The design method is efficient and the CPU time is marginally above that of a pure analysis calculation.

Euler flow solver

The MultNas flow code[9,10] is a multiblock multigrid method of classical Jameson[1,11] type. It has a cell centred finite volume discretization approach advancing asymptotically in time using local time-steps in a Runge-Kutta fashion to drive the explicit solution to steady state. In the present application it is run in Euler mode only.

Let ρ be the density, V=(*u, v, w)* the velocity in the coordinate directions and *E* the total energy per unit volume and unit mass. The solution vector then is

$$\boldsymbol{U} = (\rho, \rho u, \rho v, \rho w, \rho E)^T \qquad (7)$$

For the generally written Euler equations

$$\frac{\partial \boldsymbol{U}}{\partial t} + \nabla \Pi = 0 \qquad (8)$$

with the tensor Π incorporating the convective and impulsive pressure terms, the finite volume formulation for a small cell with volume *VOL* can now be expressed as

$$\frac{\partial \boldsymbol{U}}{\partial t} VOL + C(U) - D(U) = 0 \qquad (9)$$

C(U) denotes summations of convective fluxes and pressure, respectively, over cell surfaces. *D(U)* is the artificial dissipative term. The artificial dissipation can be of scalar isotropic or anisotropic types, where the blend of second and fourth order terms is controlled by a pressure sensor switch. The integration in time is performed using a Runge-Kutta time-stepping scheme. Let *r*(U) denote the driving right hand side flux residual of the discretized equations.

$$r(U) = -C(U) + D(U) \qquad (10)$$

With time step Δt the algorithm for a *k*-stage Runge-Kutta scheme can be symbolically written as

$$\begin{aligned} U^0 &= U^{n-1} \\ U^i &= U^0 + \alpha_i \Delta t r(U^{i-1}), \; i = 1, \ldots, k \\ U^n &= U^k \end{aligned} \qquad (11)$$

for the *nth* iterative step. The constants α_i are conveniently chosen. For a five stage scheme good performance is e.g. obtained using

$(\alpha_1, \alpha_2, \alpha_3, \alpha_4, \alpha_5) = (0.25, 0.167, 0.375, 0.5, 1.0)$

Local time steps as well as multigrid techniques are available for convergence acceleration to steady state.

Optimization method

The simple structure of the linear relation between pressure and contour variations in Eq (1) and its numerical approximation Eq (4) give rise to the question whether such a relation could be used in an optimization procedure involving drag. If this could be the case at least in an approximate redesign operation such a module would be easy to append to an analysis code just like the inverse module. The solution of a non-linear problem takes many time steps to reach steady state so the sparse updating of the

geometry will take negligible time. The problem with non-linear flow equations is to find the linear correction relation between pressure and geometry that has physical or mathematical relevance or preferably both properties, but still is simple enough for the attempted application. In linear flow models, like panel methods, there usually exists such a relation via an aerodynamic influence coefficient matrix[13]. However, in non-linear flow this is not the case. What is available in an iterative procedure is the consecutive pressure output response from the solver on a commanded geometry input correction. This information is suggested to be used to establish a temporary approximate relation similar to Eqs (1) and (4) by successively fitting the unknown parameter coefficients.

An attempt to build an optimization procedure so far in 2D based on such a pressure geometry correction relation will be outlined and some preliminary results will be shown.

Preliminaries

As an introduction to quadratic shape optimization with constraints the Sears-Haack optimal drag body in linear supersonic flow was numerically recovered by discretizing the classical wave drag integral[12] . In short the integrand of the drag integral, containing the logarithmic kernel multiplied twice by the 2nd derivative of the cross sectional area, was discretized using central differences. The objective function was made up of the drag and the Lagrange multiplier constraints for volume and centre of gravity. Differencing the quadratic form of the objective function with respect to discrete node areas and multipliers led to the solution of a linear system of equations. With 60 nodes covering the unit length and with unit body volume the area distribution came out as in Fig 8. It compares well with the analytical body. Using a 386 PC computer with 16 bit representation, the drag was 3.7 % lower than the analytical figure[12]. In the following a quadratic shape optimization module using Lagrange multipliers will be suggested.

Simple linear discrete relations like Eq(4) lead to quadratic expressions exclusively in z_i when writing down the drag surface pressure integral of an airfoil. Now drag optimization suggests itself by requiring 1st order derivatives of the drag with respect to the temporary design variables z_i to be zero to have a stationary optimized solution. This will result in linear system of equations for the unknown corrections z_i . In more general engineering applications constraints containing imposed lift, wing volume or thickness etc can easily be added utilizing Lagrange multipliers λ_i . Still the optimization procedure will result in the solution of linear system of equations for the design variables z_i and the multipliers λ_i.

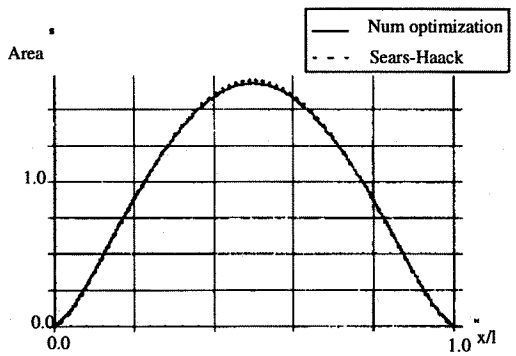

Fig 8. Axisymmetric body from quadratic optimization of wave drag at constant volume in linear supersonic flow.

Lagrangian formulation

Introduce the set of wing boundary design variables $B = \{B_k\}$ and consider the Lagrangian $\mathcal{L}$ subject to lift constraint $L=L_t$

$$\mathcal{L}(B,\lambda) = w_1 \oint_S dD + w_2 \frac{1}{2} \oint_S \left(P - P_t\right)^2 ds + \lambda \left(\oint_S dL - L_t \right) \quad (12)$$

Here D is drag and L denotes lift while P is the pressure. Subscript $(\ )_t$ is indicating target and (w_1,w_2) are weight fractions in the objective part of $\mathcal{L}$ and λ is the multiplier. S symbolizes the airfoil line integral circuit around the airfoil of unit chord. With proper normalisation D, L and P can be substituted by coefficents C_D, C_L and Cp respectively. On perturbing around the current temporary state the differential drag and lift increments come out to be

$$dD = \left(P_c + p\right)\{\left(dZ_c + dz\right)\cos\alpha - dX\sin\alpha\} \quad (13)$$

$$dL = -\left(P_c + p\right)\{\left(dZ_c + dz\right)\sin\alpha + dX\cos\alpha\} \quad (14)$$

Here α is the angle of attack and subscript $(\ )_c$ indicates current values. Perturbations are denoted by p and z. When the frame of reference (X,Z) is oriented so that $\alpha = 0$, it follows that Eq (14) is linear in all perturbation quantities. Hence, Eq (12) is quadratic and bilinear in p, z and λ . In this situation the necessary optimality conditions symbolically are

$$\frac{\partial \mathcal{L}}{\partial B} = w_1 \oint_S \frac{\partial}{\partial B}(dD) + w_2 \oint_S \left(P - P_t\right)\frac{\partial p}{\partial B} ds + \lambda \oint_S \frac{\partial}{\partial B}(dL) = 0 \quad (15)$$

$$\frac{\partial \mathcal{L}}{\partial \lambda} = \oint_S dL - L_t = 0 \quad (16)$$

, where

$$P - P_t = p + \left(P_c - P_t\right)$$

Now, assume there exists a known linear approximation relation between perturbations p and z such that

$$p = \mathcal{A}z \tag{17}$$

$\mathcal{A}$ is some linear operator. Furthermore, assume the linear geometry parametrization of the perturbation z exists

$$z = \mathcal{F}(X;B) \tag{18}$$

Then the system Eqs (15)-(16) will be given the solution (B, λ). The set of surface design variables B then is defining the new parametrized geometry correction z in an iterative process like that sketched in Fig 7.

In the following an attempt to use the simple structure of the MGM ansatz Eq (1) as closure condition for the system Eqs (15)-(16) will be outlined. Then assume the operator $\mathcal{A}$ of relation Eq (17) to have the general structure

$$\mathcal{A} = \mathcal{F}_0 + \mathcal{F}_1\frac{\partial}{\partial x} + \mathcal{F}_2\frac{\partial^2}{\partial x^2} \tag{19}$$

, where $\mathcal{F}_i(x) = f_i\, h_i(x)$ and $i = 0, 1, 2$. The coefficients f_i have convenient values and h_i are modulating functions. For the discretization of Eq(17) on the grid x_i, make the simple choice of Eq (18) to give B_i such that

$$B_i = z_i(x_i) \tag{20}$$

, where index i is numbering the discrete nodes x_i on the airfoil. With these assumptions Eqs(15) -(16) can be solved for the unknown geometry corrections z_i in all nodes.

Quadratic shape optimization method

By discretizing Eqs (13)-(19) on x_i using the design variables z_i from Eq(20), a quadratic shape optimization module named QUSHOP was set up. This led to the following discretized set of linear equations

$$\sum_i \left[w_1\frac{\partial}{\partial z_k}dD_i + w_2\left(p_i + P_c - P_t\right)\frac{\partial p_i}{\partial z_k}dX_i + \lambda\frac{\partial}{\partial z_k}dL_i \right] = 0$$

$$\sum_i dL_i - L_t = 0 \tag{21}$$

,where $i=1, n$ and n is the number of grid points, while z_k is the considered design variable with $k = 1, n$. The same discrete model as for inverse design gives p_i in terms of z_i

$$p_i = a_i z_{i-1} + b_i z_i + c_i z_{i+1}$$

The surface panel discretization goes like

$$dZ_i = Z_{i+1} - Z_i \;;\; dX_i = X_{i+1} - X_i$$

In short, using the above discretization in system Eq(21) , the linear system for solving the design perturbations z_i and the multipliers λ_j can be arranged on a general matrix form

$$\begin{bmatrix} A & C \\ C^T & 0 \end{bmatrix}\begin{bmatrix} \bar{z} \\ \bar{\lambda} \end{bmatrix} = \bar{r} \tag{22}$$

, where A is a penta-diagonal nxn matrix stemming from the pure objective part of Eq (12), while matrix C has dimension mxn. C is originating from the constraints and m is the number of constraints. In this case is $m=1$. The design solution vector is $\bar{z} = (z_k)$ with $k=1, n$. The multipliers are found in vector $\bar{\lambda} = (\lambda_j)$ with $j=1, m$. The right hand side is $\bar{r} = (r_i)$, where $i=1, n+m$. For the Lagrangian $\mathcal{L}$ to have an absolute minimum with respect to the physical design variables (z_k) a sufficient criterion is that A in Eq (21) should be positive definite. This has implications on the choice of the operator $\mathcal{A}$ and its discretization.

Hence, in summary, by appending the outlined optimization module to the Euler analysis code and by sparsely updating the airfoil geometry using Eq (22) an iterative procedure for redesign has been created as illustrated in Fig 7.

The factors (f_0, f_1, f_2) in operator $\mathcal{A}$ can successively be evaluated by a least square fit connecting the *previous surface correction* with its subsequent *flow solver pressure correction answer* to the commanded geometry correction. Hence the operator $\mathcal{A}$ can be re-evaluated by minimizing the objective function $\mathcal{G}$ as follows

$$\mathcal{G} = \oint_S \left\{\left(P - P_c\right) - \left(\mathcal{F}_0 z + \mathcal{F}_1 z' + \mathcal{F}_2 z''\right)\right\}^2 dS$$

$$\frac{\partial \mathcal{G}}{\partial f_i} = 0 \;,\; \text{where } \mathcal{F}_i = f_i\, h_i(x) \text{ and } i = 0, 1, 2.$$

The modulating functions $h_i(x)$ are structurally being suggested from differential perturbation considerations of the flow equations resulting in the use of fairly local information. The approximation of $\mathcal{A}$ should be as simple as possible. This to keep the method attractive with the objective to enable the appending of the optimization module to existing analysis solvers at minor additional computational cost.

Before up-dating the wing geometry, $Z = (Z_c + z)$, the correction z is under relaxed. This is also the case when updating the coefficients (f_0, f_1, f_2).

Computational Results

Inverse 3D wing design

Within the cooperative European LARA research and development programme, an unknown 17° swept wing was distributed in terms of planform and target Cp pressure distributions at constant spanwise wing sections. The transonic Mach number was specified to M=0.75 and the angle of attack for the geometric base line configuration was set to

α=1°. The initial baseline airfoils building the wing were all the symmetric NACA 0012 and there was no wing twist.

For the above test case Saab prepared a C-H finite volume grid containing 257x33x37 nodes in the *i, j* and *k*-directions respectively, see definitions in Fig 5. An analysis solution was first established. After that the inverse design mode was switched on. The inverse design mode was applied every 10th multigrid cycle. Generally a good approximation to the target pressure was obtained within 10 design steps , see e.g. the residual Rms of ΔCp shown in Fig 16. However, to come to the fine details more design iterations were needed especially for the wing root and tip regions. Results in Figs 9-14 are displayed after 100 design cycles and 1000 multigrid cycles.

Fig 9 is showing the isobar pattern on the upper side of the transonic wing, while Fig 10 is illustrating the very good agreement achieved between target and designed pressures at semi-span stations 30%, 50% and 80% . In the same stations the airfoil geometry comparison with the true geometry is shown in Fig 11. Even here the agreement is astonishingly good. However, good agreement with the target pressure signature in one section does not automatically guarantee good agreement with the true airfoil geometry. This is revealed in the root section shown in Fig 12. In spite of the agreement with regard to pressure fairly large disagreements in airfoil coordinates were obtained on the lower side. However, still the agreement regarding curvature, which is a sensitive parameter, is surprisingly good which can be seen at the bottom of Fig 12.

Now moving outboard to 90% semi-span, the agreement with target data is still very good with respect to both pressure and geometry including curvature. However by looking at the spanwise wing twist distribution shown in Fig 14, the 90% station is seen to be in the region where comparatively large twist deviations occur away from the true geometry. This twist discrepancy is probably due to the spanwise grid resolution being too coarse to resolve the tip flow correctly. Wing twist deviations can locally be seen in the root region too, although not as pronounced as in the tip region. Attempts to cluster spanwise grid lines locally in the root and tip regions can be seen in Fig 15. However it is felt that the present grid resolution still has to be increased to properly recover the true twist distribution in the tip and wing root regions.

Some introductory studies were carried out to see how the inverse design method would behave in supersonic flow. A slightly different generic test case was defined at *Mach 2* in which the mission was set to redesign a given symmetric wing (Fig 17) to obtain a specified target span load distribution *CL * C* at constant lift, see Fig 18 .

The design rules for the supersonic case were formulated so as to keep the shape of the chordwise pressure difference ΔCp between lower and upper sides the same as with the base line wing but locally scale it up or down during the design process to create the specified target load distribution. To build the temporary target *Cp* the scaled chordwise ΔCp distributions were then centred around the *Cp* mean value of upper and lower wing sides obtained with the base line configuration. In this way new upper and lower target *Cp* distributions were successively created keeping the symmetric mean part fixed while successively scaling the asymmetric *Cp* part. With linear thin-wing theory one could then expect the resulting airfoils to have the same thickness distributions as the initial base line wing but with a twist distribution appropriate for the imposed span load distribution. This was approximately confirmed in the numerical design calculations using the non-linear equations.

The imposed supersonic target load distribution was of elliptic type, see Fig 18. A two block C-H grid having 193x25x49 grid nodes was created. The generic base line wing-body configuration (Fig 19) was built by symmetric NACA sections with relative thickness ranging from 3-6%. The initial base line test case at Mach 2 and $\alpha = 4^{\circ}$ was computed using the Euler analysis mode. After having run the inverse design mode the obtained span loading is in general fairly close to the elliptic target distribution as shown in Fig 18. However, a slight obstruction is seen at the wing outboard leading edge kink position as well as comparatively large deviations inboard close to the vertical symmetry plane. The corresponding twist distribution seen in Fig 19 would create practical problems when trying to loft the wing geometry. This is due to the limited degree of freedom allowed for by using twist only and no wing camber. Nevertheless, the present exercise indicates that the inverse method also works in supersonic flow and to a moderate cost. The results in Figs 18-19 were obtained after 600 Euler multigrid cycles and 40 design iterations.

In conclusion the inverse design method has been demonstrated to work in a number of 3D cases, here ranging from transonic to supersonic flow, but in other applications also down to Mach 0.2. It can equally be used in viscous flow because the surface pressure is the only input. Redesign in 2D has been performed using Navier-Stokes equations. The method is fairly robust and inexpensive and can be appended to any non-linear analysis code. The overhead cost on top of one analysis calculation is very moderate.

What remains to improve on, having a more far reaching automization in mind, is the selection and updating procedure of the coefficients and functions contained in the residual correction equation. Work on this is ongoing in connection with the quadratic shape optimization method.

2D Shape optimization

A feasibility study has started in 2D to see whether an optimization method could be developed using a simple pres-

sure-contour relation similar to the residual correction equation in the inverse design method. To use an inverse method efficiently requires some skilled experience. Using an optimization method, minimizing an objective function, global aerodynamic quantities like drag, pitching moment or lift combined with geometric constraints can be controlled. Some preliminary results will here be shown using the Lagrangian $\mathcal{L}$ defined in Eq (12) as an objective function with added lift constraint only. So far it was thought to be sufficient for demonstration to use only one constraint although for instance additional requirements like given volume or thickness can easily be implemented. This will be done in coming work efforts.

The first demonstration is shown in Fig20 where an inverse design case was formulated like an optimization problem for given target Cp_t with $w_1 = 0$ and $\lambda=0$ in Eq(12). The target was created by running a *NACA0012* airfoil in Euler analysis mode at *Mach 0.85* and $\alpha = 2^o$. The initial start solution with the same airfoil and Mach number was computed at $\alpha = 0^o$. The upper part of Fig 20 shows the logged cost function ($\mathcal{L}$) and lift (*CL*) versus the number of optimization cycles. After a slight overshoot with the integrated *CL*-value a reasonably good solution is reached after about 70-80 correction steps. This is also confirmed by looking at the achieved *Cp* pressure signatures at the bottom of Fig 20.

The second case to be illustrated, Figs 21-22, is a redesign optimization of the *RAE2822* airfoil with respect to wave drag subject to constant *CL* . The operation is carried out at *Mach 0.73* starting at $\alpha=2^o$ with the target lift constrained to *CL=0.82*. The weight fractions of the Lagrangian $\mathcal{L}$ were set to $w_1 = 1$ and $w_2 = 10^{-4}$ respectively. At the bottom of Fig 22 the cost function as well as aerodynamic forces *CD* and *CL* are consecutively logged versus iteration number . After about 150 optimization cycles the cost function and aerodynamic forces have levelled out. The pressure distribution in the upper part of Fig 22 is indicating an increased rear loading which is confirmed by the new airfoil geometry shown in the middle of Fig 22. The absolute airfoil thickness is reduced by about 10%. The drag *CD* has come down from 0.0092 to 0.0063 a reduction of about 32%. Decreasing drag by reducing thickness is trivial but to do so at constant *CL* may not be so trivial. The final *CL*-value is ending up at 0.8183 which is about 0.5% too low compared to target. In Fig 21 the global Rms time history is shown versus multigrid cycles.

The present introductory study has produced some interesting results. The method is potentially flexible and fairly general objective functions can be constructed. Aerodynamic and geometric constraints can easily be incorporated by inclusion of Lagrangian multipliers. A developed method will be inexpensive and the autonomous optimization module can easily be connected to existing analysis flow solvers. Future development efforts will lie in the pressure contour relation ansatz.

Conclusions

A method for 3D inverse wing design has been presented and demonstrated in transonic and in supersonic flow. Some preliminary studies in aerodynamic optimization have been carried out in 2D trying to generalise some of the inverse ideas into a redesign method using quadratic shape optimization. The inverse method have in general shown very good results in comparison with target objects. It has demonstrated to be an inexpensive versatile numerical tool for wing design. The introductory optimization efforts have given some interesting results. Future work should be devoted to the linear perturbation relation between pressure and wing geometry. This will also benefit the inverse design method. What makes both methods attractive is that they are inexpensive to apply. The optimization formulation makes side constraints easy to add. Both methods rely on fairly autonomous modules that can be connected to existing analysis solvers.

Acknowledgement

Part of this work was carried out within the LARA programme sponsored by the European Commission / DGXII (APAS Contract, Aero CT-92-0054). The inverse transonic wing geometry was made available by Daimler Benz Aerospace Airbus in Bremen and the target pressure was computed by DLR in Braunschweig. The Swedish funding was partly made possible by NUTEK (Contract 5226-92-04971P) whose support is greatly appreciated.

References

1. Frontiers of Computational Fluid Dynamics- 1994. Ed. D.A. Caughey & M.M. Hafez. 1994 J. Wiley & Sons Ltd. Chichester-NewYork-Brisbane-Toronto-Singapore.
2. Livne E. Multidisciplinary design optimization. Aero Space America, Dec 1994.
3. Computational Methods for Aerodynamic Design (Inverse) and optimization. AGARD-CP463. March 1990.
4. Optimum Design Methods for Aerodynamics. AGARD Report 803. Nov 1994.
5. Malone J.B., Narramore J.C., Sankar L.N., Airfoil design method using the Navier-Stokes equations. J. of Aircraft, Vol 28, No 3, pp. 216-224, 1990.
6. Garabedian P., McFadden G., Design of supercritical swept wings. AIAA J. Vol 20, pp. 289-291, March 1992.
7. Larsson T., Sedin Y. C-J., 3D Wing design method using the Euler flow equations. LARA Techn Rep No 02. APAS Contract Aero CT-92-0054. Saab MA Febr 1994.
8. Larsson T., Sedin Y. C-J., Inverse transonic wing design. LARA Techn Rep No 27. APAS Contract Aero CT-92-0054. Saab MA Nov 1994.
9. Sedin Y. C-J., Nävert G., Ålund A., Transonic flow calculations using approximate potential and Euler equations. Mathematics and Computers in Simulation 29 (1987), pp. 503-514.
10. Lötstedt P., Sillen M., Multigrid multiblock solver of the stationary Euler and Navier-Stokes equations. Saab MA Rep L-0-R164 part II, April 1996.

11. Jameson A., Full-potential, Euler, and Navier-Stokes Schemes. Progress in Aeronautics and Astronautics. Ed Seebass A.R., AIAA 1990, pp. 39-88.
12. Ashley H., Landahl M., Aerodynamics of Wings and Bodies. Addison-Wesley 1965.
13. Woodward F.A., Analysis and design of wing-body combinations at subsonic and supersonic speeds. J. Aircraft Vol 5, June 1968, pp 528-534.

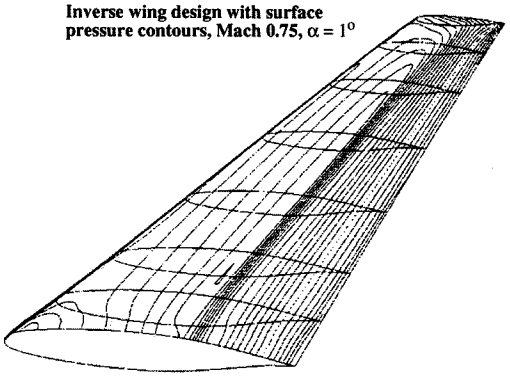

Fig.9. Designed wing with pressure contours at Mach 0.75 and $\alpha = 1^{o}$. Initial start of inverse design process using NACA 0012 wing.

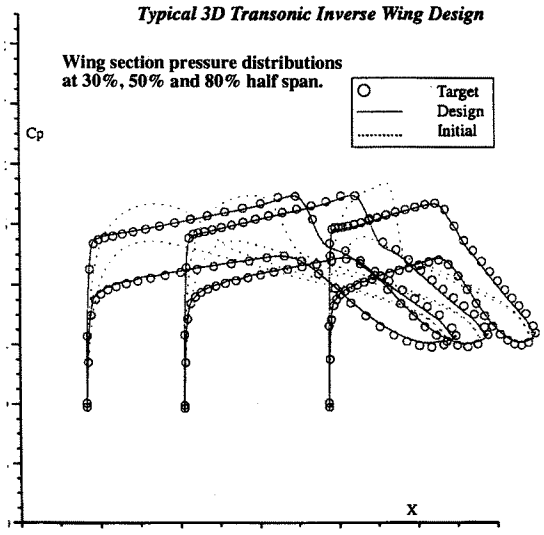

Fig 10. Pressure distributions of designed wing and of target object at semi-span stations 30 %, 50 % and 80 % . Mach 0.75 and $\alpha = 1^{o}$. Initial start NACA 0012 wing.

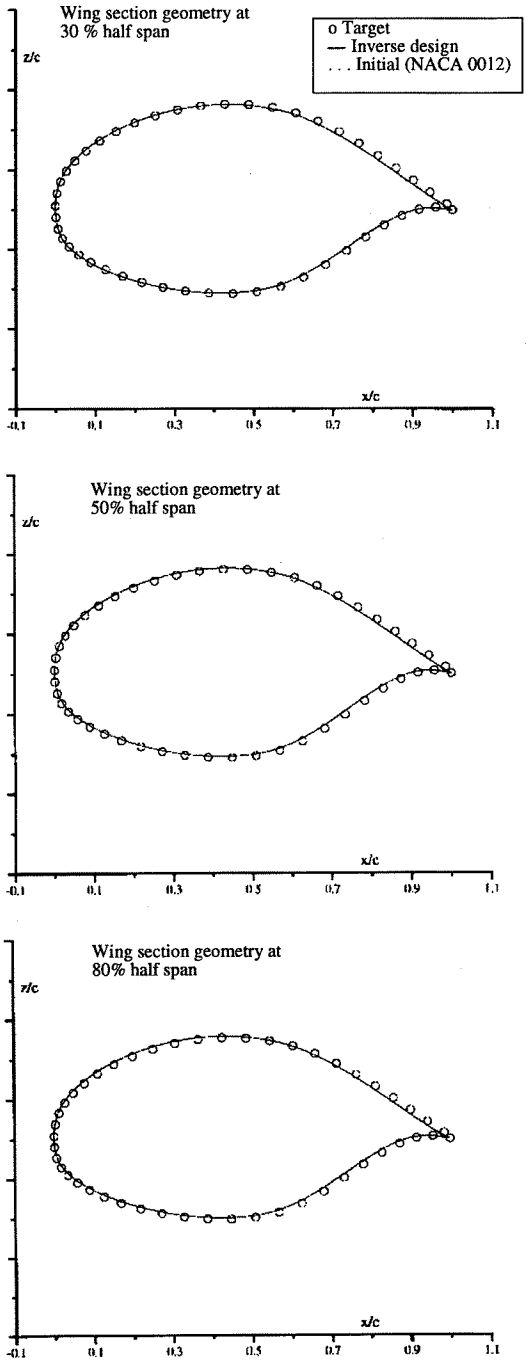

Fig 11. Wing geometry of inverse design and "unknown" target object at 30%, 50% and 80% semi-span stations. Mach 0.75 and $\alpha = 1^{o}$. Initial start NACA 0012 wing.

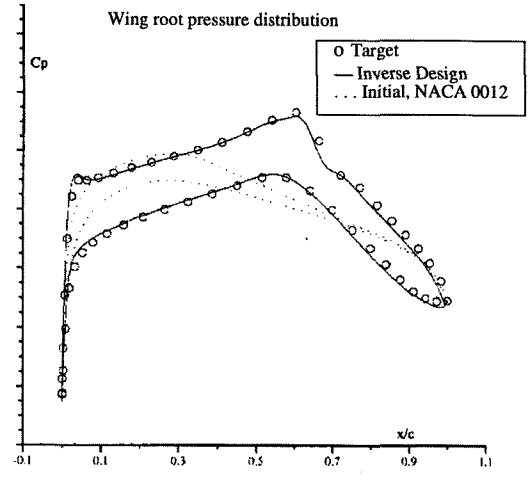

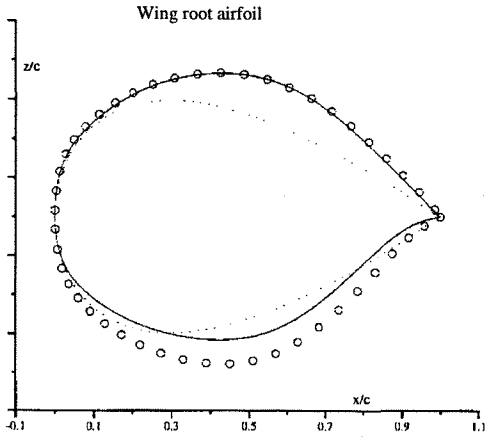

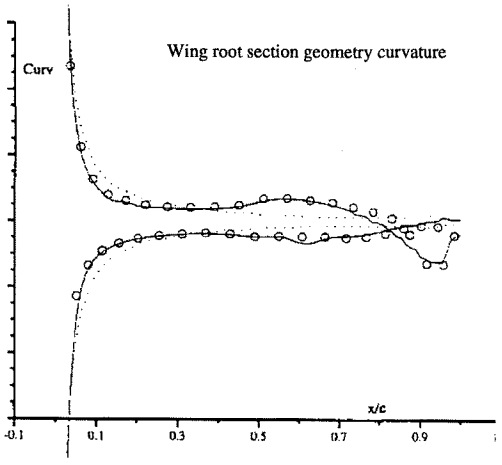

Fig 12. Pressure distribution, airfoil geometry and curvature of 3D inverse designed wing and "unknown" target in root symmetry plane (0% semi-span). Mach 0.75 and $\alpha = 1^{o}$. Initial start NACA 0012 wing.

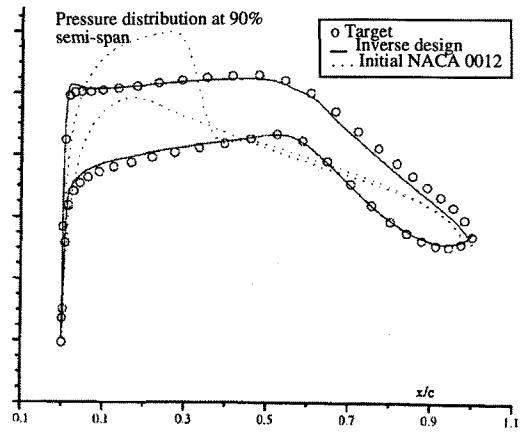

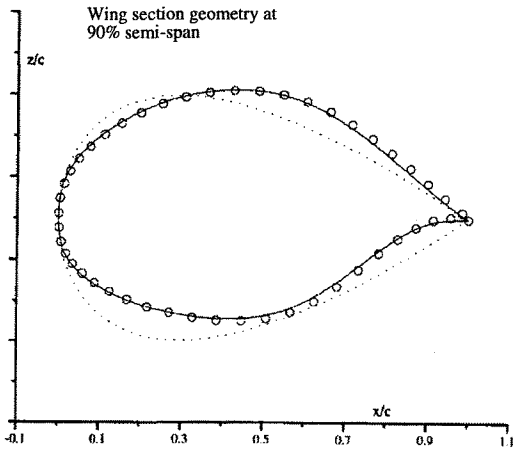

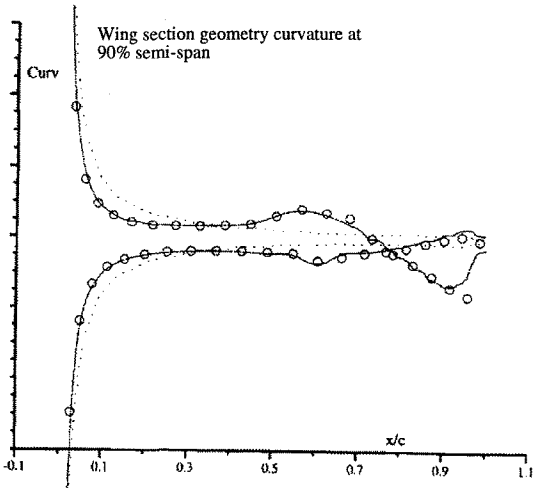

Fig 13. Pressure distribution, airfoil geometry and curvature of 3D inverse designed wing and "unknown" target at 90% semi-span. Mach 0.75 and $\alpha = 1^{o}$. Initial start NACA 0012 wing.

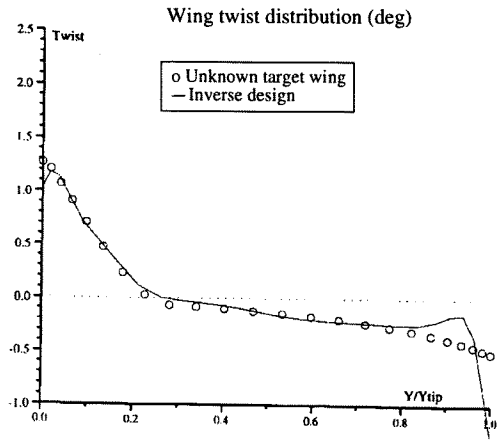

Fig 14. Comparison of twist distribution between designed wing and "unknown" target object. Mach 0.75 and $\alpha = 1^{o}$.

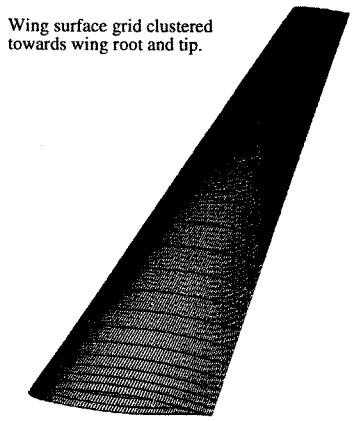

Fig 15. Spanwise grid clustering at root and tip of 3D inverse designed wing. Mach 0.75 and $\alpha = 1^{o}$

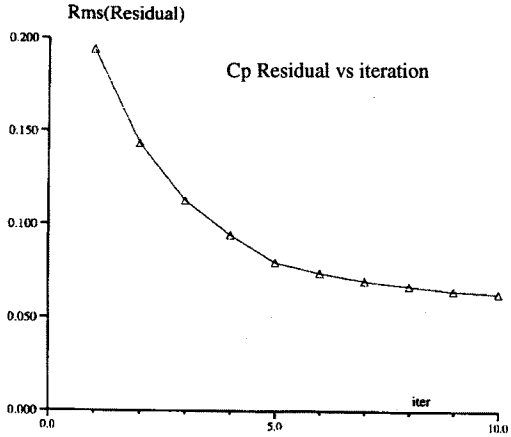

Fig 16. Rms(Cp Residual) vs design iteration of inversely designed wing at Mach 0.75 and $\alpha = 1^{o}$. Geometry up-date at every 10th multigrid cycle.

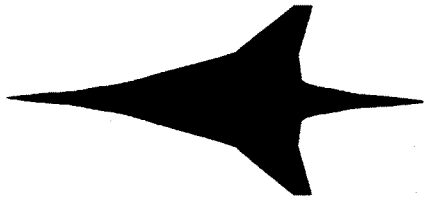

Fig 17. Supersonic configuration.

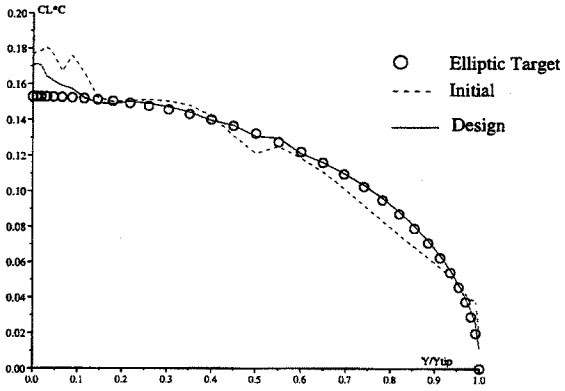

Fig 18. Span load distribution of supersonic configuration, Mach 2 and $\alpha=4^{o}$. Target, initial and obtained CL*C.

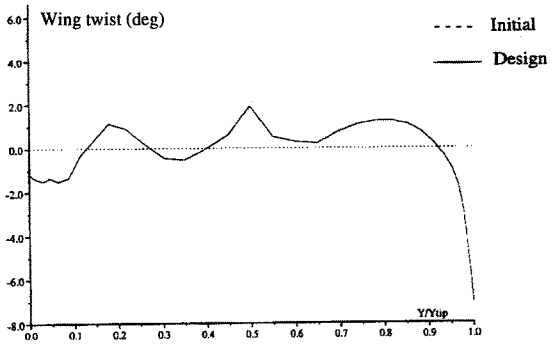

Fig 19. Wing twist distribution of supersonic configuration. Mach 2 and $\alpha=4^{o}$. Designed and initial distributions.

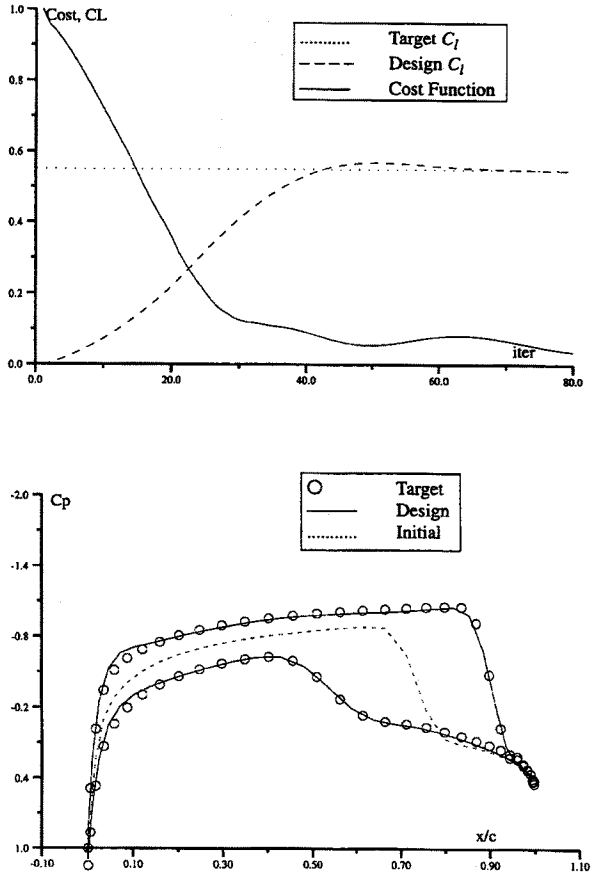

Fig 20. 2D Inverse design formulated as an optimization problem. Target *Cp* from *NACA 0012* at *Mach 0.85* and $\alpha=2^o$. Initial solution from *NACA 0012* at *Mach 0.85* and $\alpha=0^o$. No constraint on *CL*. Upper part: evolution of cost function and *CL* ; lower part: *Cp*-distributions of target, design and initial solutions.

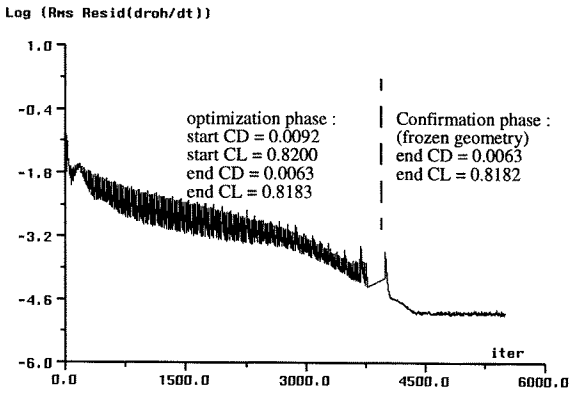

Fig 21. Rms flow residual of 2D wave drag optimization vs multigrid cycle, starting with *RAE2822* at *Mach 0.73*, $\alpha=2^o$. Constrained *CL* = *0.82*. Geometry up-date every 20th multigrid cycle.

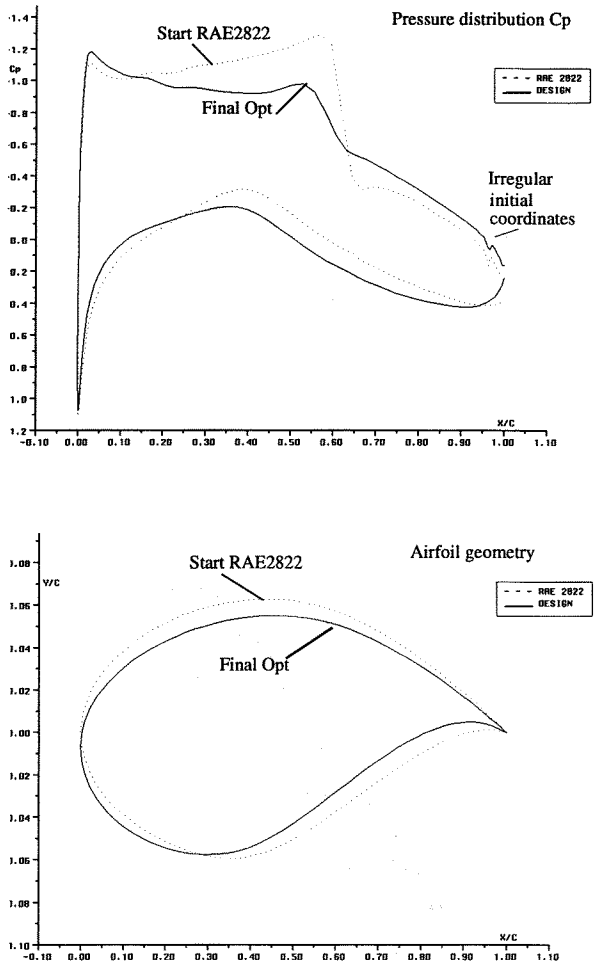

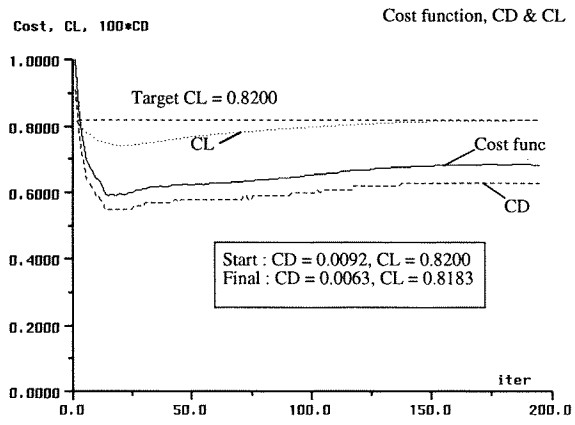

Fig 22. 2D Airfoil wave drag optimization starting with *RAE2822* at *Mach 0.73*, $\alpha = 2^o$. Constrained lift : *CL=0.82*. Upper part- pressure distribution *Cp* ; middle part- airfoil geometry ; lower part- cost function and aerodynamic forces *CL, CD* vs. design iteration number. Geometry up-date every 20 th multigrid cycle.